

Production of low-Sn Cu-Sn Alloy Coatings onto Steel Substrate Using Sodium Citrate Bath – Part 1: the Effect of Current Mode (DC or SPC) and Applied Current on the Chemical, Morphological, and Anticorrosive Properties of the Coatings

Nathalia Xiaohui Zhou^a, Priscila Santos da Silva^a , Antônio Vitor de Castro Braga^a,
Dalva Cristina Baptista do Lago^a, André Rocha Pimenta^b , Lilian Ferreira de Senna^{a*} 

^aUniversidade do Estado do Rio de Janeiro (UERJ), Instituto de Química, Laboratório de Eletroquímica e Corrosão (LEC), Rua São Francisco Xavier, 524, Pavilhão Haroldo Lisboa da Cunha, S. 427, Maracanã, 20550-013, Rio de Janeiro, RJ, Brasil.

^bInstituto Federal de Educação Ciência e Tecnologia do Rio de Janeiro (IFRJ), Laboratório de Instrumentação e Simulação Computacional, Campus Paracambi, Rua Sebastião de Lacerda, Fábrica, 26600-000, Paracambi, RJ, Brasil.

Received: January 26, 2022; Revised: June 23, 2022; Accepted: July 25, 2022

This work reports the production of low-tin Cu-Sn alloy coatings on carbon steel substrates using a bath containing CuCl_2 , SnCl_2 , and sodium citrate. In the first part of this study, the coatings were electrodeposited by direct and simple pulse current processes (DC and SPC, respectively). Different current density values were used, while the pulse frequency and duty cycle remained constant. Independent of the current mode used, low-tin Cu-Sn coatings, showing globular surface morphology and Cu_6Sn_3 as the main compositional phase, were produced. Both the current mode and the applied current density affected the anticorrosive properties of the coatings. The most protective DC and SPC coatings, showing Sn content < 3 wt.% and compact morphology, were prepared using $j = 80 \text{ A m}^{-2}$ and $j_c = 167 \text{ A m}^{-2}$, respectively. High charge transfer resistance values were verified even after immersion for 24 h in 0.5 mol L^{-1} NaCl solution.

Keywords: *Cu-Sn alloy, cyclic voltammetry, DC process, SPC process, sodium citrate, anticorrosive coatings.*

1. Introduction

Functional metallic coatings are widely used to enhance the hardness, mechanical, and anticorrosive properties of the substrate material, making them feasible for several industrial applications¹. The use of metallic alloys as functional coatings presents the advantages of combining the properties of different metals in a single material, which makes it more attractive than pure metal coatings². Cu-Sn alloy coatings, for example, can be used in microelectronics, aerospace, and automotive sectors, as well as for decorative artifacts. Each application, however, requires several different characteristics, which are generally obtained by varying the composition of the alloying elements. The amount of Sn in the coating often affects important alloy properties such as ductility, corrosion resistance, weldability, and low surface tension directly^{3,4}.

Commercially, electrodeposition processes (galvanostatic or potentiostatic) are usually the main routes for producing metal coatings. The galvanostatic process deposition is commonly chosen to be used industrially because the applied current can easily control the mass of deposited films, according to Faraday law. Also, the chemical composition of the coatings generally varies with the applied current

density, which may affect the morphology of the coatings and their corrosion resistance⁵.

Galvanostatic electrodeposition can be performed by applying direct or pulsed current (DC and PC, respectively). As DC electrodeposition is a usual and low-cost process, it is the most used current mode to produce metallic alloy coatings⁶. Other current modes, such as simple and reverse pulsed current (SPC and RPC, respectively), have also been applied to electrodeposit metal alloy coatings in plating industries. Generally, the PC deposition processes produce films with smaller grain sizes, enhanced adhesion, lower porosity, and superior electrochemical behavior compared to those prepared using DC process^{7,8}. As the variation in the PC electrodeposition parameters (the cathodic pulse current density, j_c ; the anodic pulse current density, j_a ; the cathode pulse duration, t_{on} ; and the anodic pulse duration, t_{off}) affects the mass transport situations and the surface phenomena that can occur in a PC deposition process, coatings with different properties may be produced^{9,10}. However, depending on the deposition condition applied to produce the DC coatings, these layers may also be free of cracks and defects¹¹, presenting properties comparable to those prepared by PC electrodeposition.

The production of metallic alloy coatings by DC or PC electrodeposition processes requires the simultaneous

*e-mail: lsenna@uerj.br

reduction of all the metallic ions in solution on the surface of the electrode, which is not a task usually so simple to achieve. The deposition of both alloying elements is promoted by adding a complexing agent to the electrolytic bath, which may form complexes with the ions in the solution and alter the kinetics of the reduction reactions. Besides, the complexing agents may alter the electrochemical potential of the species and prevent precipitation and displacement reactions¹²⁻¹⁴. Cu-Sn coatings have already been obtained commercially using electrolytic baths containing cyanides, fluoroborate, boron-fluorides, and phosphates, as complexing agents¹⁵⁻¹⁷. However, these species can be harmful to human beings and aggressive to the environment. Alternative, environmentally friendly complexing agents, such as citrates, glycinates, methanesulfonic acid, and tartrates, have already been studied for other Cu-alloy coatings^{2,4,18} and for producing Cu-Sn alloy coatings^{5,6,11,13} by electrodeposition technique. Sulfuric acid solutions containing several different additives have also been studied for this purpose^{3,19}.

Among the alternative baths, those based on methanesulfonic acid and sodium citrate have produced Cu-Sn coatings showing interesting properties^{6,11,13,20,21}. Most works concerning methanesulfonic acid deal with Cu-Sn films prepared using the DC process only^{20,21}. However, Zanella et al.¹¹ produced Cu-Sn coatings on low alloy carbon steel by DC and SPC using a metanesulfonic acid bath and compared the effects of both deposition processes on the chemical and morphological characteristics of the Cu-Sn coatings. Although only one j_c value was applied, the authors observed that by keeping the duty cycle constant, an increase in the pulse frequency from 0.1 Hz to 10 Hz influenced the composition of the film, increasing the amount of copper and allowing the appearance of different phases of the alloying elements. It was also found that the corrosion resistance of the coatings in 0.1 mol L⁻¹ NaCl solution decreased under the same conditions and that the DC coating presented a corrosion current density value smaller than those obtained for the high-frequency SPC coatings.

Besides its low toxicity and ability to complex several metallic ions, citrate is also known for its leveling and brightening action²², mainly in several copper alloy deposition processes, which have been widely discussed in the literature²³⁻²⁶. Tin alloys are also deposited from citrate-containing baths using both DC and PC deposition processes, producing alloys with different morphologies and remarkable properties²⁷⁻²⁹. Although the electrodeposition of Cu-Sn alloy using citrate-based baths and DC processes is relatively well known in the literature^{6,30,31}, only a few works can be found using PC processes and this complexing agent to produce bronze coatings^{32,33}. Furthermore, no studies compare the anticorrosive properties of Cu-Sn coatings produced by both DC and PC processes from a citrate bath.

Based on the absence of literature data concerning the development of anticorrosive Cu-Sn coatings produced by the SPC process and using a citrate bath, as mentioned above, it is necessary to perform a detailed investigation of this topic. Therefore, the first part of this study compares the anticorrosive properties of DC and SPC Cu-Sn alloy coatings produced using an electrolytic bath containing sodium citrate as a complexing agent. The applied current

density was varied in both deposition processes, while the applied frequency (F) and duty cycle (γ) were maintained constant for the SPC deposition experiments. By using inductively coupled plasma optical emission spectrometry (ICP-OES), scanning electron microscopy (SEM), energy dispersive spectroscopy (EDS), X-ray diffraction (XRD), and electrochemical impedance spectroscopy (EIS), the present study aimed to verify the effects of the current mode (DC or SPC) and the applied current density on the chemical contents, morphological aspects, and the anticorrosive properties of Cu-Sn coatings electrodeposited on carbon steel substrate from a citrate bath. Also, the conditions selected in this work will be further used in Part 2 to verify the effects of duty cycle and pulse frequency on the properties of these coatings.

2. Experimental Procedures

2.1. Electrodes and electrolytic bath

This section describes the electrodes and electrolytes used in the electrochemical experiments shown in this work. Two different electrodes were used as working electrodes in the experiments described in this section, and the pretreatment used in each case will be presented.

Graphite electrodes (0.286 cm² area) were used in the cyclic voltammetry experiments. These electrodes were sanded with 600 mesh granulometry sandpaper, washed with deionized water and ethyl alcohol, and dried with warm air before immersion in the voltammetric cell.

The electrodes used as substrates in all of the electrodeposition experiments (section 2.3) were AISI 1020 carbon steel disks with an exposed area of 4.9 cm². These disks were sanded with emery paper (100 to 600 mesh), polished with alumina grade no. 2, degreased with an alkaline lauryl sulfate bath, and washed with deionized water and ethylic alcohol. Finally, the disks were dried with warm air and immersed in the electrolytic bath.

In both cyclic voltammetry and electrodeposition experiments, the counter electrode was a Pt spiral, while the reference electrode was a saturated calomel electrode (SCE). The Pt electrode was immersed in 20%v/v HNO₃ solution for 1 minute, immediately before being used in the experiments, to remove any oxide layer that could be present. The SCE electrode was washed with deionized water and dried with soft paper.

The solutions used in the electrochemical tests (sections 2.2 and 2.3) are presented in Table 1. The pH of the solutions was adjusted to near 6.00, with NaOH 1.00 mol L⁻¹.

The anticorrosive experiments were performed in a 0.5 mol L⁻¹ NaCl electrolyte (pH = 7.06). The solutions presented in this section were prepared using pure grade reagents (>99.99%) and deionized water.

2.2. Cyclic voltammetry experiments

The cyclic voltammetry tests were performed in duplicate series, using Solutions 1 to 3 of Table 1, without stirring. A potentiostat/galvanostat AUTOLAB PGSTAT302N was employed in these experiments, and the electrochemical cell contained three electrodes: the working electrode (graphite electrode), the saturated calomel reference electrode (SCE), and a platinum spiral as the counter electrode. The scanning

Table 1. Chemical composition and pH values of solutions used in electrochemical tests.

Solution	CuCl ₂ .2H ₂ O (mol L ⁻¹)	SnCl ₂ .2H ₂ O (mol L ⁻¹)	Sodium citrate (mol L ⁻¹)	pH
1	0.2	-	0.5	5.63
2	-	0.02	0.5	5.65
3	0.2	0.02	0.5	6.00

rate used in the voltammetry tests was 10 mVs⁻¹ and the potential varied from 1 to -1.6 V, returning to 1 V (SCE).

2.3. Electrodeposition experiments

The electrodeposition experiments were carried out in triplicate series only in Solution 3 of Table 1, under constant stirring conditions (300 rpm) and at room temperature (25 °C). In the electrochemical cell used in these experiments, the carbon steel disk was the working electrode, a Pt spiral was the counter electrode, and SCE was the reference electrode. The coatings were produced using the same potentiostat/galvanostat AUTOLAB PGSTAT302N to apply direct current (DC) or simple pulsed current (SPC). Six current density (*j*) values were chosen to produce the Cu-Sn alloys on the steel substrate: 10 A m⁻², 50 A m⁻², 80 A m⁻², 100 A m⁻², 150 A m⁻², and 200 A m⁻². Based on Faraday law, each electrodeposition time was calculated to produce a 10 mg coating.

In the SPC electrodeposition process, the cathodic peak current densities (*j_c*) were calculated using Equation 1, where *j_m* is the average current density. In the present work, the chosen *j_m* values used in SPC deposition were the same selected for *j* in DC deposition. The current-on time (*t_{on}*) and the current-off time (*t_{off}*) were obtained from Equation 2, where *γ* is the duty cycle.

$$j_m = j_c \times \frac{t_{on}}{t_{on} + t_{off}} \quad (1)$$

$$\gamma = \frac{t_{on}}{t_{on} + t_{off}} \times 100\% \quad (2)$$

In the first part of this work, the SPC coatings were produced using *γ* fixed at 30% and the pulse frequency (*F*) at 1000 Hz. This *γ* value was chosen because it is usually used for Cu and Cu-alloys coatings deposited by SPC¹⁰. On the other hand, using such a high *F* value may create a transport condition in the double layer that could be very different from that found when DC was used. Thus, it would be possible to verify differences in the chemical composition of the coatings produced by DC and SPC deposition processes and the effects observed in this property due to the current variation. The same conditions used here have already been applied for Cu-Co alloy coatings produced by the group, with satisfactory results³⁴. The deposition conditions for producing the DC and SPC coatings are shown in Table 2.

The mass of the produced layers was obtained by weighting the working electrode, before and after the deposition, in analytical balance (SARTORIUS TE214S, ±0.1 mg error). This mass was used to calculate the cathodic current efficiency value (*E_p*). After weighting, the layers were dissolved in 20%v/v HNO₃, and the alloy composition was determined by inductively coupled plasma optical emission spectrometry (ICP-OES) using a THERMO SCIENTIFIC iCAP 6000 SERIES equipment. These results were used to

Table 2. Conditions used to produce the electrodeposited Cu-Sn coatings using DC and SPC modes.

DC		SPC*		
Experiment	<i>j</i> (A m ⁻²)	Experiment	<i>j_m</i> (A m ⁻²)	<i>j_c</i> (A m ⁻²)
1	10	1'	10	33.3
2	50	2'	50	167.0
3	80	3'	80	267.0
4	100	4'	100	333.3
5	150	5'	150	504.1
6	200	6'	200	667.0

* *F* = 1000Hz; *γ* = 30%; *t_{on}* = 0.3ms; *t_{off}* = 0.7ms

obtain the average content of each metal in the coatings, as the %wt. Cu and %wt. Sn.

The deposited mass (*m_{deposited}*) was also used to calculate the thickness of the coatings (*h*), using Equation 3.

$$h = \frac{m_{deposited}}{A\rho_c} \quad (3)$$

where *ρ_c* is the density of the coating (g cm⁻³), considering the contents of Cu and Sn in each deposited coating, while *A* is the electrode area (4.9 cm²).

2.4. Characterization of Cu-Sn coatings

2.4.1. Morphological analysis

The effects of the current density and the electrodeposition process (DC or SPC) on the surface morphology of the Cu-Sn coatings were evaluated by scanning electron microscopy (SEM) using a JEOL JSM G510 LV microscope and a secondary electron detector (SE). The analysis was carried out in a high vacuum and secondary electron mode, using a voltage of 20 kV.

SEM also visualized the cross-sections of the Cu-Sn coatings showing the best anticorrosive results. A wire electrical discharge machining (wire-EDM) was used to section the samples, and the cut was made to permit the cross-section analysis of the center, avoiding the end of the samples. After this procedure, the samples were embedded in acrylic resin and sanded (220 to 1200 grinding paper) to be analyzed on a HITACHI TM3000 microscope, operating at 15 kV and backscattered electron (BSE) mode. In the BSE mode, areas with greater atomic weight chemical elements show lighter gray tones, while those with lower atomic weight exhibit darker gray tones. Elemental analyses were also performed using an energy dispersive spectroscopy (EDS) detector model X-Flash Min SVE (BRUKER) coupled to the SEM. The EDS results were present in EDS maps, where each chemical element is associated with a color. This technique allows for evaluating the distribution of the chemical elements along the region.

2.4.2. Phase identification analysis

The phase identification of the Cu-Sn coatings' components was performed by X-ray diffraction (XRD), using a diffractometer RIGAKU ULTIMA IV and the software MATERIALS DATE JADE 5 XRD pattern processing. The Cu-K α radiation ($\lambda = 1.5406 \text{ \AA}$), at 40 kV was used and the 2θ ranged from 10° to 90° , at a scanning rate of 0.020 s^{-1} .

The experimental 2θ values, which were used to calculate both the d (hkl) parameters of the diffraction lines and the full width at half maximum (FWHM), were obtained by fitting the more prominent diffractogram lines of the Cu-Sn coatings using a Gaussian equation (using Microcal Origin®, release 8.0). As the FWHM of the X-ray diffraction line is related to the apparent size of the particles³⁵, this parameter was used to evaluate the apparent size of the crystallites using Equation 4:

$$d_p = \frac{k\lambda}{\beta \cos\theta} \quad (4)$$

where d_p is the crystallite size, k is a constant related to the type of the crystal structure, λ is the wavelength of the incident radiation (nm), and β is the FWHM³⁵.

2.4.3. Electrochemical characterization

All electrochemical characterizations were performed without stirring and in a naturally aerated solution. Electrochemical impedance spectroscopy (EIS) experiments were carried out to verify the anticorrosive ability of the Cu-Sn coatings produced on the steel substrate under the conditions described in section 2.3. The experiments were performed in duplicate at 25°C , in 0.5 mol L^{-1} NaCl solution, using a three-electrode cell, in which the coating/substrate systems were used as the working electrodes, a platinum spiral was the counter electrode, and a saturated calomel electrode (SCE) was the reference electrode. The same potentiostat/galvanostat AUTOLAB PGSTAT 302N was used to perform these experiments.

After a potential stabilization of approximately 1h, the EIS evaluations were performed at the open circuit potentials, in a frequency range of 10^5 to 10^{-3} Hz and amplitude of 10 mV. The Cu-Sn/steel substrate systems presenting the best anticorrosive performances were also evaluated by EIS after 24 h of exposure in the same aggressive medium, using the same frequency range and amplitude value.

The EIS data were fit using the NOVA 1.10 software (METROHM AUTOLAB). The values of the double layer electrical capacitance (C_{dl}) were calculated from the admittance of the constant phase element (Y) using Equation 5³⁶:

$$C_{DL} = (Y)^{\frac{1}{N}} \times R \left(\frac{1}{N} - 1 \right) \quad (5)$$

where N is the term that defines the equivalence degree of the constant phase element for a capacitive component and R is calculated by Equation 6³⁶, considering R_s as the electrolyte resistance and R_{ct} as the charge transfer resistance:

$$R = \frac{R_s R_{ct}}{R_s + R_{ct}} \quad (6)$$

Based on the EIS results, polarization curves were performed in the coating/substrate systems that presented the best anticorrosive performances, using the same potentiostat/galvanostat, corrosive medium, and electrolytic cell earlier described. The linear voltammetry experiments were carried out after potential stabilization (approximately 1 h), and the potential ranged from -0.5 V_{SCE} to 0.5 V_{SCE} around the open circuit potential, with a scanning rate of 1 mV s^{-1} , at 25°C . The corrosion current density (j_{corr}) and the corrosion potential (E_{corr}) values of the selected coating/substrate systems were obtained by Tafel extrapolation.

3. Results and Discussion

3.1. Cyclic voltammetry

Figure 1 shows the voltammetric results for the graphite substrate in the solutions presented in Table 1. When the graphite electrode was immersed in Solution 1, in which only Cu (II) species and citrate ions were present, two broad reduction peaks, at approximately -0.418 V (C_1) and -1.127 V (C_2), were observed. A sharper peak is also noted at more negative potentials, which can be related to the reduction of hydrogen reaction (HER) from water.

According to the literature^{32,37}, the hydrogenated citrate compounds (denominated Cu(II)-CitH complex in the present work) predominate in solutions where citrate concentration

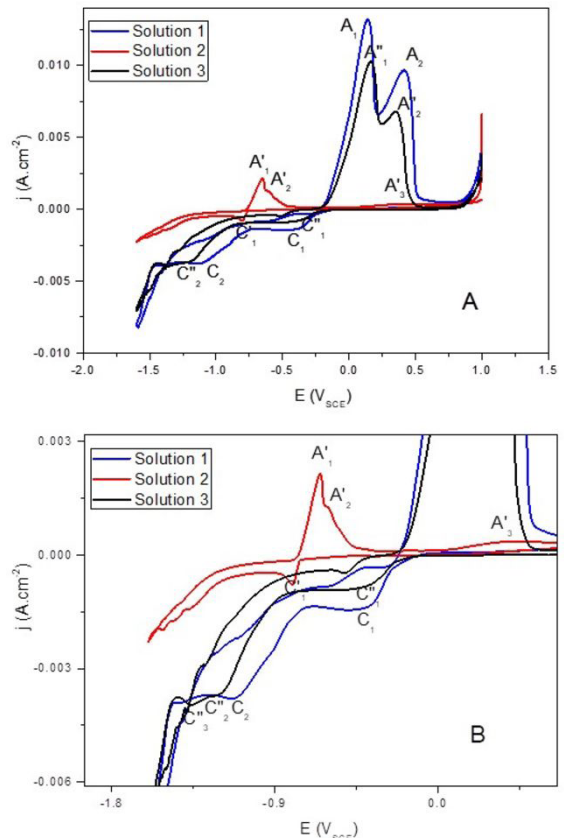


Figure 1. (A) Cyclic voltammetry for graphite in the solutions of Table 1; (B) Magnification of the cathodic branch.

ranges between 0.5-0.8 mol L⁻¹, at a pH range similar to that used in the present work. Based on the most accepted reduction mechanism^{22,38}, the C₁ peak may be related to the reduction of the Cu(II)-CitH complex to the Cu(I)-CitH complex. This monovalent complex is adsorbed on the graphite surface, blocking a fraction of the electrode area and causing the polarization observed in the voltammetric curve (Figure 1B). The second electron transfer may occur at C₂ via adsorbed monovalent copper intermediate. In the anodic branch of this curve, two oxidation peaks were verified. The anodic peak A₁ (0.146 V) corresponds to the oxidation of Cu (0) to Cu (I) species, while the peak A₂, observed in more positive potentials (0.413 V), is related to the oxidation of Cu (I) to Cu (II) species^{15,38}.

The voltammetric curve for the substrate in Solution 2 shows the reduction process of Sn (II) ions in the presence of citrate. It is observed that the reduction potential of the Sn (II)-citrate complexes in the graphite electrode is shifted to more negative values when compared to the reduction potential of the Cu (II) ions. This result indicates that the reduction of Sn (II) in a bath containing sodium citrate may be more difficult than that of Cu (II) ions. A cathodic peak C'₁ at -0.804 V (more clearly observed in Figure 1B) is present in the curve related to Solution 2. Considering that the probable complex formed in the studied pH is the Sn(II)-CitH species, the reduction of Sn (II) to Sn (0) would occur, after the previous dissociation of this complex, as proposed by Han et al.³⁹.

In the anodic branch, three oxidation peaks were observed. The A'₁ peak (-0.648 V) suggests the formation of a passive layer of SnO or Sn(OH)₂, while the shoulder A'₂ (-0.605 V) is probably related to the formation of a passive layer of Sn(OH)₄^{40,41}. Another oxidation peak (A'₃) was verified at more positive potentials (0.390 V). This peak was preceded by a region of low current intensity, which corresponds to a passive state and, once again, may be related to the electroformation of species containing Sn (IV)⁴².

Figure 1 also shows the voltammogram of the graphite substrate immersed in the solution containing both Cu (II) and Sn (II) ions and sodium citrate (Solution 3). This curve is similar to that obtained when the substrate was immersed in the medium containing only Cu (II) and citrate (Solution 1). The potential of the C''₁ peak (-0.392 V), observed in the curve for the graphite immersed in Solution 3, is close to the potential of the first peak verified for the substrate in Solution 1 (-0.418 V). Nevertheless, this result indicates that the reduction of the divalent copper complex to the monovalent one occurred at less negative potentials in a bath containing Sn (II) ions. At more negative potentials, there are two peaks, C''₂ (at -1.220 V) and C''₃ (at -1.370 V), which may be related to the reduction of both the adsorbed Cu(I)-CitH complex and the dissociated Sn (II) ions, respectively. Although both peaks were shifted to more negative potentials when the electrode was immersed in Solution 3, compared to the curves using Solutions 1 and 2, it is interesting to note that a more significant potential dislocation was observed for the Sn (II) reduction peak. The simultaneous presence of Sn

(II) and Cu (II) species in a simple electrolytic bath usually facilitates the reduction of Cu (II) to metallic copper by Sn (II). Choosing a proper complexation agent may avoid this problem. However, in the present work, the reduction of Sn (II) ions was probably hindered in Cu (II) presence. As the stabilization constants (K_f) for the Cu(II)-citrate complex (1.58 X 10⁵)²² is lower than that found for the Sn(II)-citrate complex (3.16 X 10¹⁹)⁴³ and using a Cu (II):Sn (II) ratio = 10:1, the voltammetric results indicate that the reduction of Cu (II) ions will be facilitated.

During the anodic sweep, two oxidation peaks, A''₁ (0.165 V) and A''₂ (0.354 V), were verified. These values can be compared with those obtained for the substrate in the baths containing the isolated ions (Solutions 1 and 2). Although shifted to more positive values, the potential of the A''₁ peak is close to the value of the A₁ peak, observed for the curve of graphite in Cu (II) and citrate medium (0.146 V), which may suggest the oxidation of metallic copper. On the other hand, the potential of the A''₂ peak is shifted to less negative potentials, compared to both A₂ (0.413 V) and A'₃ (0.390 V) peaks, related to the curves of the electrode in Solutions 1 and 2, respectively. Although the A''₂ peak position is closer to the A'₃ peak potential, its high current intensity value may recommend that the oxidation of Cu species cannot be discarded under this condition. Therefore, it can be suggested that A''₂ may be related to the oxidation of both metals.

The results of cyclic voltammetry on the graphite electrode indicate that the Cu-Sn alloys formed under the conditions used in this work are likely low-tin alloys.

3.2. Electrodeposition of Cu-Sn coatings

Table 3 presents the main average results obtained for the DC and SPC coatings produced by electrodeposition using the conditions described in Table 2. The color of the coatings varied from bright red to yellow reddish depending on the deposition condition used. All the coatings were adherent to the carbon steel substrate (qualitative observation), independent of the current mode applied.

The average values of cathodic current efficiency (E_c) are above 80% (except for the condition obtained at j = 150 A m⁻² in the DC process). This result indicates that most of the applied current density was used in the deposition process, whereas parallel reactions consumed less than 20% of this parameter. On the other hand, average E_f values above 100% were obtained when the j = j_m = 10 A m⁻² was used. This result could be related to the entrapment of the monovalent Cu-citrate complex, adsorbed on the steel surface as mentioned in the voltammetric evaluation (Section 3.1), during the electrodeposition process. Although similar results were obtained by Chaissang, Quang, and Wiart⁴⁴, new experiments are still needed to reach a conclusion about this topic.

During the electrodeposition process, the reduction of Cu (II) and Sn (II) ions is controlled by their consumption on the substrate surface. After this stage, reduction depends on the transport of the species from the solution to the surface.

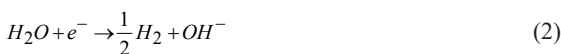
Table 3. Average values \pm standard deviation (sd) of current efficiency (E_f , %), calculated thickness (h , μm), and copper and tin contents (%wt. Cu and %wt. Sn) in the coatings produced at different j values (Table 2), using DC and SPC.

Exp. ^(a)	$E_f \pm \text{sd}$ (%)	$h \pm \text{sd}$ (μm)	Cu \pm sd (%wt.)	Sn \pm sd (%wt.)	Exp. ^(b)	$E_f \pm \text{sd}$ (%)	$h \pm \text{sd}$ (μm)	Cu \pm sd (%wt.)	Sn \pm sd (%wt.)
1	101 \pm 1.2	2.30 \pm 0.03	99.98 \pm 0.10	*	1'	101 \pm 2.6	2.32 \pm 0.15	99.34 \pm 0.57	*
2	91 \pm 6.2	2.08 \pm 0.19	99.02 \pm 0.21	1.00 \pm 0.13	2'	100 \pm 2.0	2.29 \pm 0.13	97.20 \pm 0.20	2.80 \pm 0.41
3	98 \pm 1.0	2.24 \pm 0.08	97.59 \pm 0.15	2.41 \pm 0.18	3'	100 \pm 1.6	2.29 \pm 0.11	97.80 \pm 0.29	2.20 \pm 0.26
4	86 \pm 4.9	1.98 \pm 0.12	94.37 \pm 0.11	5.62 \pm 0.12	4'	100 \pm 1.2	2.34 \pm 0.27	96.09 \pm 0.98	4.70 \pm 0.13
5	57 \pm 2.6	1.32 \pm 0.08	91.97 \pm 0.15	7.50 \pm 0.29	5'	95 \pm 1.6	2.19 \pm 0.05	94.51 \pm 0.04	5.45 \pm 0.11
6	88 \pm 2.0	2.02 \pm 0.08	96.89 \pm 0.14	3.09 \pm 0.18	6'	82 \pm 2.0	1.88 \pm 0.06	97.87 \pm 0.11	2.13 \pm 0.11

^(a) Exp.1 ($j = 10 \text{ A m}^{-2}$); Exp.2 ($j = 50 \text{ A m}^{-2}$); Exp.3 ($j = 80 \text{ A m}^{-2}$); Exp.4 ($j = 100 \text{ A m}^{-2}$); Exp.5 ($j = 150 \text{ A m}^{-2}$); Exp.6 ($j = 200 \text{ A m}^{-2}$). ^(b) Exp.1' ($j_c = 33.3 \text{ A m}^{-2}$); Exp.2' ($j_c = 167.0 \text{ A m}^{-2}$); Exp.3' ($j_c = 267.0 \text{ A m}^{-2}$); Exp.4' ($j_c = 333.3 \text{ A m}^{-2}$); Exp.5' ($j_c = 504.1 \text{ A m}^{-2}$); Exp.6' ($j_c = 667.0 \text{ A m}^{-2}$).

* The Sn concentration in the ICP analysis was below the detection limit

It causes a cathodic polarization process and improves Reactions 1 to 4, depending on the electrolyte pH.



Under the conditions of the present study, where the pH of the electrolyte used was around 6.00, the most likely parallel reaction observed due to the electrode polarization was HER (Reaction 2). This parallel reaction is enhanced at more negative potentials, as seen in Figure 1.

As the current density shifts to more cathodic values in DC processes, the substrate surface is polarized and the HER prevails, which can be verified by the E_f values. For example, in the case of Experiment 5 ($j = 150 \text{ A m}^{-2}$), around 43% of the current density was consumed by this reaction. Besides, the increase in the HER leads to the alkalization of the interface. It may cause the precipitation of metals hydroxides on the surface of the electrode and contribute to the weighted mass value obtained⁴⁵. The precipitation process can be related to the increase in the average E_f value shown in Experiment 6, performed at $j = 200 \text{ A m}^{-2}$, compared to that presented in Experiment 5.

When the E_f values for the coatings obtained by DC and SPC deposition modes are compared, it is possible to note that, in the majority of the experiments, the coatings produced by SPC presented $E_f \approx 100\%$, suggesting that in the simple pulsed current electrodeposition all of the applied current density was used in the deposition process. This result can be explained by reminding that, in the DC process, the negatively charged layer formed around the cathode during the electrodeposition progression is charged at a defined thickness, hindering the solution ions from reaching the electrode surface. On the other hand, as in the SPC electrodeposition the current is periodically switched off, this layer can be partially discharged, allowing the ions to reach the electrode surface more easily. Thus, in the SPC process, the concentration of the metallic ions close to the cathode, which decreases after a high deposition rate during the current application time (t_{on}), can be recovered by ion

migration, diffusion, and convection during the current-off time (t_{off})^{34,46}. This effect is reflected by E_f maintenance of around 100% for most of the SPC coatings, as verified in Table 3. Therefore, the parallel processes are decreased in the SPC electrodeposition, and a reduction in the E_f value was observed only at the highest applied cathodic current value.

Almost all of the produced coatings presented calculated thickness values (h) of approximately $2 \mu\text{m}$, as seen in Table 3. The main exception can be verified for the coating produced under the conditions of Experiment 5 ($j = 150 \text{ A m}^{-2}$; DC), which presented the lowest E_f value and, consequently, the lowest average h value ($1.32 \pm 0.08 \mu\text{m}$). As a whole, many differences among the thicknesses of the coatings obtained from either the DC or the SPC electrodeposition processes were not observed. However, when the coatings are compared for the same j (or j_m) value, those prepared using the SPC process presented higher average h values than the DC-produced coatings, except for $j = j_m = 200 \text{ A m}^{-2}$. As the thickness values were obtained using Equation 3, these results are directly related to the deposited mass values, which were higher for the SPC coatings.

Table 3 also presents the average results for the elements' contents in the coatings, as %wt. Cu and %wt. Sn, obtained for each experimental condition presented in Table 2. Independently of the current mode used (DC or SPC), the %wt. Cu values were higher than the %wt. Sn. These results confirm that low-Sn coatings were produced in this work, as proposed by the voltammetric curves presented in Figure 1. Additionally, only under the conditions of $j = 100$ and 150 A m^{-2} (Experiments 4 and 5, respectively - DC process) and $j_c = 333.3$ and 504.1 A m^{-2} (Experiments 4' and 5', respectively - SPC process), the %wt. Sn values obtained in this work were approximately similar to or higher than that in commercial bronze (95%wt. Cu - 5%wt. Sn). Moreover, when the films were produced using $j = 10 \text{ A m}^{-2}$ and $j_c = 33.3 \text{ A m}^{-2}$ for DC and SPC electrodeposition processes, respectively, the Sn concentration in these coatings was under the ICP-OES technique detection limit and was considered absent in these coatings.

The presence of a ligand in the electrodeposition bath may interfere with the alloy deposition process. It is expected that the Cu (II) reduction in a citrate bath would not occur under substrate polarization, mainly when lower current density values were applied². As the concentration of Cu (II) ions in the electrolyte (Solution 3 of Table 1) was higher than that of Sn (II) ions (Cu:Sn = 10:1), it means that the

copper deposition would be favored under these conditions, which is noted in Table 3. On the other hand, at higher current density values, the copper deposition becomes more polarized, and the reduction of Sn (II) ions would be likely enhanced. Although this behavior was verified for the DC coatings in the present work, a decrease in the Sn content was noted for the highest j value. This result is probably related to the increase in the HER process and agrees with the cyclic voltammetry experiments (Figure 1), in which the reduction of the Sn (II) ions occurred at more negative potentials than those observed for the copper deposition.

If the SPC and DC coatings are compared for the same j (or j_m) value, it can be noted that the average wt. % Sn of the SPC coatings were always smaller than those prepared using DC electrodeposition, except when $j_m = 50 \text{ A m}^{-2}$ was used. In the SPC production of alloy coatings, the resulting alloy composition can vary strongly with the applied pulse parameters (j_c , F and γ)⁴⁶. Due to the difference in the reduction potentials of the two metals, a displacement reaction occurs when the applied current pulse is switched off. Thus, the Cu (II) ions continue to reduce at the cathode during the off-time, while the less noble metal (Sn) tends to dissolve under this condition^{46,47}, which can explain the differences in the tin content present in the DC and SPC coatings.

Unlike the DC coatings, the present results do not show a direct relationship between the applied current density and the Sn content in the SPC coatings. It is known that if the off-time increases, more copper will deposit on the cathode surface until the displacement rate slows down because of the increased coverage by copper⁴⁶. However, as the parameters F and γ were maintained constant in the present experiments, the values of t_{on} and t_{off} were not changed, and only j_c was varied. Under these conditions, the alloy composition will be affected by j_c only if the Tafel slopes of the two partial reactions are different⁴⁶.

Figure 2 presents the cathodic partial polarization curves for the Cu (II) and Sn (II) reduction reactions. These curves were obtained based on the metal contents and cathodic efficiency results of the SPC experiments (Table 3), considering the j_c and the average potential values measured during the

pulse on. As a comparison, the total polarization curve is also shown. The partial curves confirm that most of the applied cathodic current density was used to reduce the Cu (II) ions, as its curve is near the total curve. Additionally, Figure 2 shows that the Tafel slopes related to both deposition processes are similar for low values of j_c . However, an intense polarization can be noted in the copper partial curve when $j_c = 333,3 \text{ A m}^{-2}$ was applied (Experiment 4'), while the effect in the tin curve was softer. From this j_c value on, the slopes of the two deposition processes are no longer similar. This result indicates that, under the condition used in the present experiments, j_c affects the deposition of both metals in the SPC process, as the polarization of the Cu (II) reduction process during the t_{on} favors the reduction of Sn (II) ions. Consequently, j_c also affects the metal composition in the coatings.

The HER influence on the SPC deposition process of the Cu-Sn coatings is observed only when the highest j_c value was applied (Experiment 6'), which is reflected by the significant change in the tin partial curve shown in Figure 2. Under these conditions, as the Cu (II) reduction process is still polarized, the H^+ reduction reaction competes mainly with the Sn (II) reduction process, causing a high decrease in the wt.% Sn value (Table 3).

3.3. Characterization of Cu-Sn coatings

This work aimed to evaluate the anticorrosive performance of the Cu-Sn coatings on a steel substrate based on their phase compositions, morphological, and electrochemical characterization. Therefore, those films prepared by both DC and SPC processes, using $j = 10 \text{ A m}^{-2}$ and $j_c = 33.3 \text{ A m}^{-2}$ (Experiments 1 and 1' for DC and SPC processes, respectively), presenting only copper in their compositions, were not characterized.

3.3.1. Morphological evaluation

The surface morphologies obtained for the selected Cu-Sn alloy coatings produced by DC and SPC electrodeposition processes are shown in Figures 3 and 4, respectively.

Independently of the current mode used to produce the coatings (DC or SPC), all coatings covered the whole substrate. Most of the coatings presented globular clusters distributed all over the surface. Few defects and cracks can also be noted. This kind of morphology is well reported in the literature for Cu-Sn alloy coatings produced by both DC and SPC electrodeposition^{11,12,32,45}.

It is possible to observe in Figure 3 that surfaces presenting cauliflower-like morphology were obtained for the DC coatings produced using 50 A m^{-2} (Experiment 2) and 80 A m^{-2} (Experiment 3) (Figures 3A and 3B, respectively). Although some cracks and defects can be seen on the surface of the coating prepared using 100 and 150 A m^{-2} (Figures 3C and 3D, respectively), the increase in the applied current density tended to produce more compact and nodular coatings, with a decrease in the size of the clusters. However, when 200 A m^{-2} was used (Experiment 6), the coating shown in Figure 3E presented a flower-like pointed structure, decreasing its compactness. This result can be related to changes in the surface energy due to the adsorption of hydrogen adatoms or hydrogen gas on the electrode, as

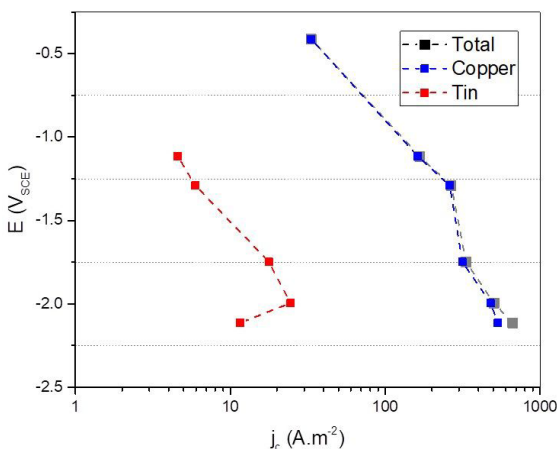


Figure 2. Partial polarization curves for copper and tin deposition during the SPC process. The total polarization curve is also presented for comparison.

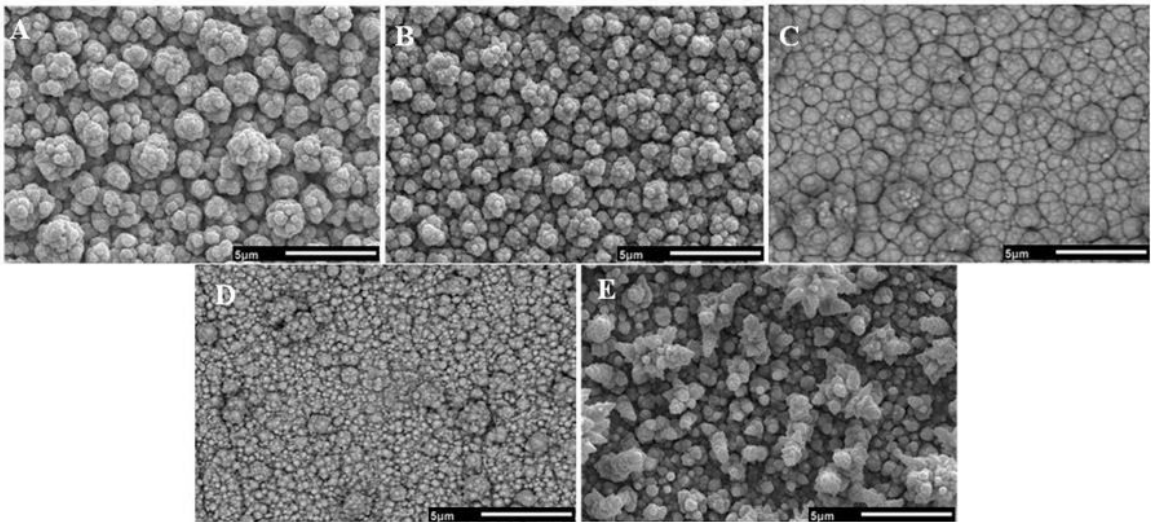


Figure 3. Surface morphology for the Cu-Sn coatings produced by DC electrodeposition, using (A) $j = 50 \text{ A m}^{-2}$ (Experiment 2); (B) $j = 80 \text{ A m}^{-2}$ (Experiment 3); (C) $j = 100 \text{ A m}^{-2}$ (Experiment 4); (D) $j = 150 \text{ A m}^{-2}$ (Experiment 5); (E) $j = 200 \text{ A m}^{-2}$ (Experiment 6). Magnification of 5000x.

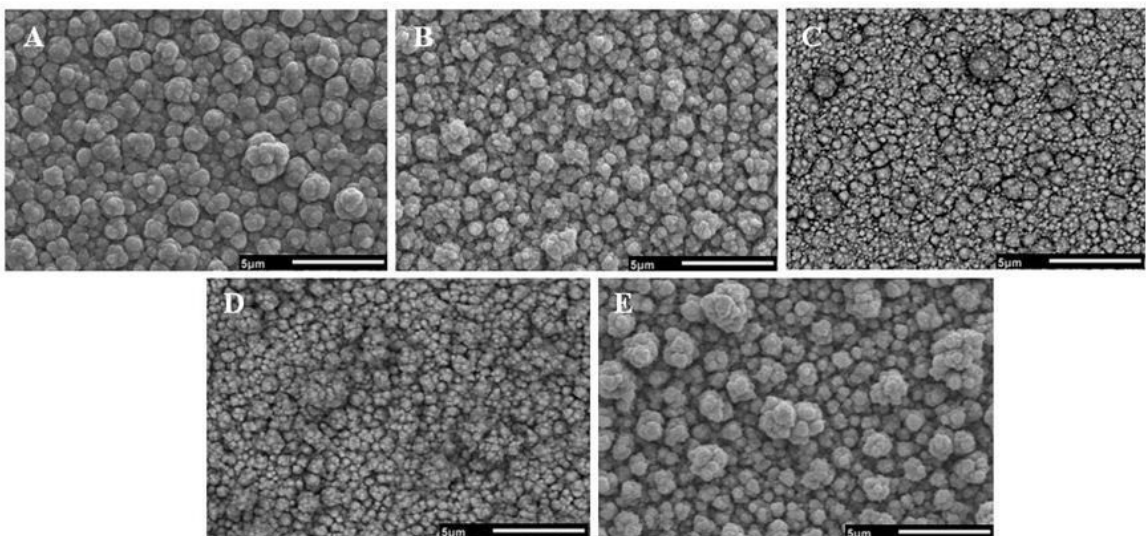


Figure 4. Surface morphology for the Cu-Sn coatings produced by SPC electrodeposition, using (A) $j_c = 167.0 \text{ A m}^{-2}$ (Experiment 2'); (B) $j_c = 267.0 \text{ A m}^{-2}$ (Experiment 3'); (C) $j_c = 333.3 \text{ A m}^{-2}$ (Experiment 4'); (D) $j_c = 504.1 \text{ A m}^{-2}$ (Experiment 5') (E) $j_c = 667.0 \text{ A m}^{-2}$ (Experiment 6'). Magnification of 5000x.

the applied current density was increased³². It is possible to verify that the DC films prepared under Experiments 3, 4, and 5 conditions (Figures 3B, 3C, and 3D, respectively) presented small clusters, which could be an interesting characteristic for an anticorrosive coating.

Similar morphologies were obtained by SPC electrodeposition, as shown in Figure 4. It was expected that the pulsed current electrodeposition would decrease the grain size and produce more refined and compact coatings than those verified when DC electrodeposition was used (Figure 3). Zanella et al.¹¹ and Meng et al.⁴⁵ found nodular microstructures when depositing Cu-Sn alloys coatings on steel substrate using SPC from metassulfonic acid bath and pyrophosphate-based bath,

respectively. This kind of microstructure is produced due to increased nucleation speed in the SPC process, enhancing the formation of a more uniform coating compared to the metallic alloy obtained by DC electrodeposition⁴⁸. Although the SPC process produced compact coatings in the present work, the differences in the morphologies among the DC and SPC coatings were not strongly marked, and a mix of nodular and globular clusters are also verified in the SPC ones. Likely, the nucleation speed of the SPC coatings was affected by the frequency value used in their production, as suggested by Zanella et al.¹¹. These authors have shown that an increase in the deposition frequency caused nodule structure and size changes, creating new clusters. Therefore,

our results suggest that the frequency value chosen for these experiments could not be suitable to produce SPC coatings showing only nodular morphologies. This hypothesis may be better evaluated in the second part of this work, in which the F and γ parameters will be varied. Nevertheless, the present study confirms that SPC electrodeposition favored the refinement of the coatings prepared from a citrate bath, as smaller clusters can be noted in these coatings.

Concerning the coatings presented in Figure 4, it is interesting to note that an almost nodular morphology is verified for the film prepared using $j_c = 504.1 \text{ A m}^{-2}$ (Experiment 5', Figure 4D). Compact coatings were also produced using $j_c = 167.0 \text{ A m}^{-2}$ (Experiment 2'), $j_c = 267.0 \text{ A m}^{-2}$ (Experiment 3'), and $j_c = 333.3 \text{ A m}^{-2}$ (Experiment 4'), as shown in Figures 4A, 4B, and 4C, respectively. However, some defects and small cracks could be detected in the coatings presented in Figures 4C and 4D, which may affect the integrity of these coatings when exposed to an aggressive environment.

3.3.2. Phase analysis

The different phases observed for the DC and SPC Cu-Sn coatings are presented in the diffractograms shown in Figure 5, while the experimental 2θ and d (hkl) values for the main diffraction lines of these coatings are displayed in Table 4. As a comparison, the corresponding d (hkl) standard values for the phases observed in the diffractograms, obtained from the database (Materials Data JADE 5 XRD pattern processing), are also shown in Table 4.

Electrodeposited films usually present a considerable distortion of the crystal lattice due to non-equilibrium phases formed on the cathode at high overpotential values. Therefore, these films consist of fine crystals, which are non-uniform in composition. Cu-Sn films produced by electrodeposition usually contain phases characteristic of the high-temperature alloy⁴⁹. Also, non-cataloged crystalline phases can be obtained in some experiments^{12,50}.

Independently of the current deposition mode, Figure 5 shows well-defined diffraction lines related to the coating (Cu-Sn phases and segregated Cu phases), indicating that crystalline films were produced. Additionally, peaks related to the steel substrate can be noted for both the DC and SPC-produced coatings, which was expected because a traditional XRD analysis was used⁵¹. All the Cu-Sn coatings present an intense diffraction line at $2\theta \sim 42.80^\circ\text{--}43.20^\circ$, which can be associated with the intermetallic phases Cu_6Sn_5 (132) (PDF n° 45-1488) and Cu_3Sn (2.10.0) (PDF n° 01-1240), as shown in Table 4. The peaks related to segregated copper phases at $2\theta \sim 43.10^\circ$, 50.17° , and 73.88° (PDF n° 04-0836), and those related to the steel substrate, at $2\theta \sim 44.50^\circ$, 64.80° , and 82.00° (PDF n° 06-0696), are also shown in Table 4.

The main difference among the diffractograms of the DC and SPC electrodeposited Cu-Sn coatings is the presence of a small diffraction peak at $2\theta \sim 36.60^\circ$ in the DC coatings produced only under the conditions of Experiments 2 and 3 (Figure 5A). This peak could be associated with the intermetallic phase Cu_3Sn (0.20.0) (PDF n° 01-1240), which has already been observed for Cu-Sn electrodeposited coatings^{11,52}. It is also interesting to observe that the relationship between the intensity of the Cu_6Sn_5 (132) line and that of the steel substrate at $2\theta \sim 44.50^\circ$ increases for the SPC coatings

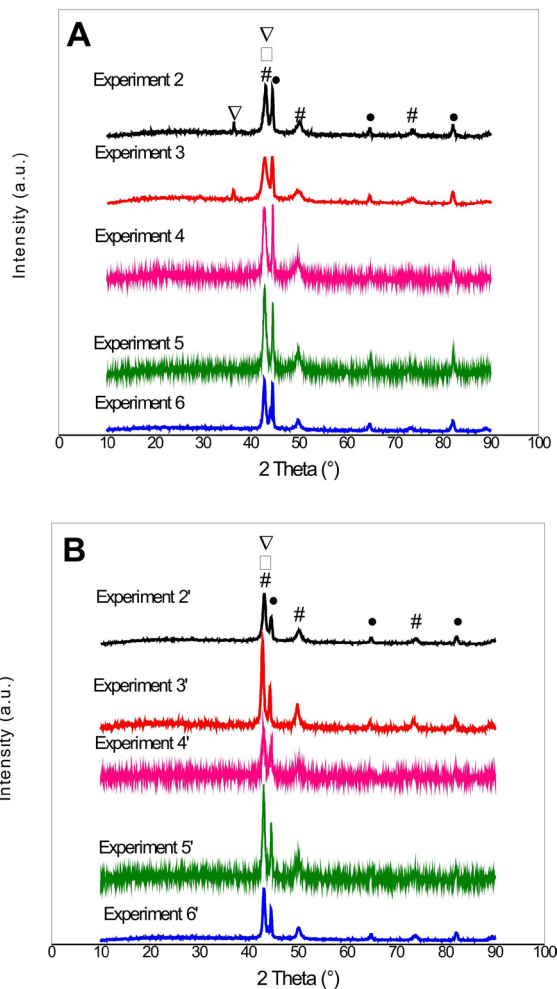


Figure 5. XRD analysis for the Cu-Sn coatings produced by (A) DC electrodeposition; (B) SPC electrodeposition. Legend of the phases: ∇ Cu_3Sn ; \square Cu_6Sn_5 ; \bullet Fe (substrate); $\#$ Cu.

compared to the DC ones suggesting that more crystalline coatings were produced by pulsed current electrodeposition.

Barbano et al.⁵² evaluated the Cu-Sn coatings electrodeposited from a bath containing EDTA and observed that the produced layers presented mainly the Cu_6Sn_5 and Cu_3Sn phases, with no Cu or Sn segregated phases. The main phase evidenced in the XRD of Cu-Sn alloys coatings produced by electrodeposition from a bath containing methanesulfonic acid was also Cu_6Sn_5 , even though Cu_3Sn and segregated Cu and Sn phases were detected in this case¹¹. A mixture of Cu and Cu_6Sn_5 phases was also verified for low-Sn Cu-Sn alloy coatings obtained from EDTA tartrate double complexing agents⁵³. The Cu_6Sn_5 intermetallic phase was also observed by Pu et al.⁷, when they produced Cu-Sn alloy anodes for lithium batteries by electrodeposition from a mixed pyrophosphate and tartaric acid medium. Therefore, the microstructural phases obtained in the present work for the Cu-Sn coating agree with the results presented in the literature.

Table 5 shows the apparent grain size for the selected coatings produced by DC and SPC electrodeposition processes, calculated using Equation 5 and based on the most intense

Table 4. $d(hkl)$ values for the Cu-Sn coatings produced by DC and SPC electrodeposition processes.

Experimentally observed values				Standard values			
DC		SPC		$d(hkl)$ carbon steel	$d(hkl)$ Cu_6Sn_5	$d(hkl)$ Cu	$d(hkl)$ Cu_3Sn
2 θ	$d(hkl)$	2 θ	$d(hkl)$				
36.60	2.460	-	-				2.380
42.93	2.106	42.79	2.108		2.103		
43.10	2.097	43.15	2.094			2.088	2.080
44.49	2.036	44.52	2.035	2.027			
50.19	1.817	50.15	1.819			1.808	
64.84	1.437	64.81	1.439	1.433			
73.88	1.282	73.88	1.282			1.278	
82.18	1.172	81.97	1.175	1.170			

Table 5. Apparent grain size calculated for selected Cu-Sn coatings produced by DC and SPC electrodeposition processes.

DC Experiment	Apparent grain size (nm)	SPC Experiment.	Apparent grain size (nm)
2	12.93	2*	13.18
3	7.04	3*	16.46
4	11.15	4*	14.60
5	13.46	5*	17.43
6	14.98	6*	16.13

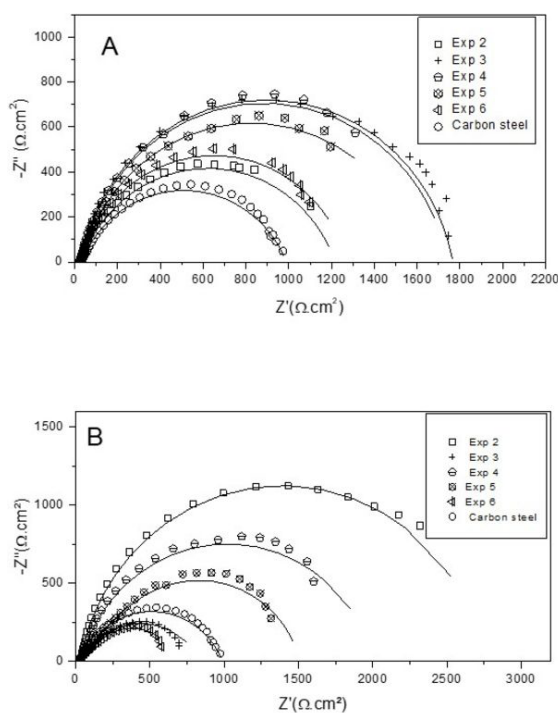
diffraction line related to the intermetallic phase Cu_6Sn_5 . The results indicate that the clusters observed in the SEM analysis (Figures 3 and 4) were formed by nanometric grains. Also, Table 5 shows that the apparent grain sizes of the DC coatings were always smaller than those produced using the SPC process for the same j (or j_m) values. This result is coherent with the increase in the crystallinity of the SPC coatings, which can be related to larger grain sizes. The smallest grain size value was verified for the coating produced under the conditions of Experiment 3 ($j = 80 \text{ A m}^{-2}$, using the DC process).

The SPC electrodeposition was expected to produce coatings with smaller grain sizes than those prepared by the DC process. However, it was not observed in Table 5. Although compact coatings were produced using the SPC process, as observed in the SEM analysis (Figure 4), the apparent size of the grains calculated for the SPC films were similar, independently of the applied cathodic pulse current used, and larger than the sizes obtained for the coatings produced by DC. According to Zanella et al.¹¹, the increase in the pulse frequency may affect the SPC deposition process and favor increasing the grain size of the coating. As this hypothesis has not been evaluated for a citrate bath yet, it will be further studied in the second part of this work. Nonetheless, the present results suggest that smaller F values should be used to decrease the size of the grains in the Cu-Sn coatings prepared by SPC.

3.4.3. Anticorrosive evaluation

Figure 6 shows the Nyquist diagrams for the DC and SPC Cu-Sn coating/steel substrate systems in 0.5 mol L^{-1} NaCl solution. The Nyquist diagram for the bare carbon steel substrate in the same electrolyte is also shown as a comparison.

In the Nyquist diagram, the diameters of the capacitive loops indicate the resistance of the systems to the corrosion process in the aggressive medium. Thus, it is possible to

**Figure 6.** Nyquist diagrams for the Cu-Sn coating/substrate systems produced by (A) DC and (B) SPC and the carbon steel in NaCl 0.5 mol L^{-1} .

observe, in Figure 6A, that the diameters of the capacitive loops for the DC-produced Cu-Sn coatings/substrate systems are higher than that of the bare carbon steel substrate. This result indicates that all the DC films can protect the substrate against corrosion. Among all the systems produced using DC, those prepared under Experiments 3, 4, and 5 conditions

($j = 80, 100, \text{ and } 150 \text{ A m}^{-2}$, respectively) showed the best anticorrosive performances. The coatings of these samples presented small globular clusters and few defects (Figure 3), and those produced under the conditions of Experiments 4 and 5 also showed average tin content similar to or higher than the value expected in commercial bronze (Table 3). These features may have influenced their anticorrosive abilities.

Concerning the SPC coatings, Figure 6B showed that only the coating/substrate systems produced using the j_c values of Experiment 2', 4', and 5' ($j_c = 167.0, 333.3, \text{ and } 504.1 \text{ A m}^{-2}$, respectively) presented anticorrosive characteristics, considering the diameter of their capacitive loops in the Nyquist diagram. All of these samples' coatings presented morphologies that can contribute to the corrosion resistance of the systems, as shown in Figure 4, and those obtained using $j_c = 333.3 \text{ A m}^{-2}$ and 504.1 A m^{-2} (Experiments 4' and 5', respectively), presented chemical composition near that verified in commercial bronze (Table 3). Thus, the electrochemical results agree with these characteristics.

The EIS results can be better analyzed using equivalent electrical circuit models, in which the values of the charge transfer resistance (R_{ct}) and the double electric layer capacitance (C_{DL}) are obtained by simulating the electrochemical data. Figure 7A illustrates the circuit used in this work to simulate the EIS data obtained for the bare carbon steel substrate, where R_s is the electrolyte resistance, R_{ct} is the charge transfer resistance, and Y represents the admittance of the constant phase element (CPE), associated with the capacitance of the electric double layer. The EIS data for the Cu-Sn coatings/substrate systems were simulated using a different equivalent circuit model, shown in Figure 7B, due to the presence of a film (the coating) on the carbon steel substrate

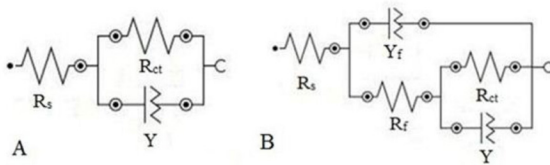


Figure 7. Equivalent circuit models used to simulate the EIS data of (A) the bare carbon steel substrate and (B) the Cu-Sn coating/substrate systems.

surface. In this case, it is considered that the first of the time constants represent the dielectric characteristics of a porous coating and the electrolyte resistance that permeate the pores (R_f-Y_f). Another circuit, parallel to this one, represents the electrode process, described by the charge transfer resistance and the capacitive characteristics present in the interface electrolyte/substrate ($R_{ct}-Y$)⁵⁴. In this circuit, R_s also refers to the electrolyte resistance.

The results obtained from the simulation of EIS data of the coating/substrate systems produced using DC and SPC electrodeposition processes are shown in Table 6. It is known that an increase in the R_{ct} and a decrease in C_{DL} values be related to coatings presenting anticorrosive characteristics^{3,55}. As the capacitance of the double electric layer is associated with the oxidation tendency of the coating/substrate system, small C_{DL} values indicate that the systems show high corrosion resistance. The C_{DL} and C_{DLf} values, also shown in Table 6, were calculated using Equation 4 (section 2.4.3).

As seen in Table 6, all the selected DC-produced coating/substrate systems present higher R_{ct} values and lower C_{DL} values than the bare carbon steel substrate, indicating that anticorrosive systems were prepared under these conditions. The Cu-Sn coating/substrate system that presented the highest corrosion resistance (highest R_{ct} and lowest C_{DL} values) was obtained using $j = 80 \text{ A m}^{-2}$ (Experiment 3). Although this coating showed a lower Sn content ($2.41 \pm 0.18\% \text{ wt.}$) when compared to the conditions obtained from Experiments 4 and 5 (5.62 ± 0.12 and $7.50 \pm 0.29\% \text{ wt. Sn}$, respectively), this behavior might have been influenced by the surface morphology of the coatings (Figure 3). While the coating produced under the conditions of Experiment 3 presented small globular clusters and no defects (Figure 3B), those prepared using $j = 100 \text{ A m}^{-2}$ and $j = 150 \text{ A m}^{-2}$ (Experiments 4 and 5, respectively) showed few defects, as can be noted in Figures 3C and 3D, respectively. The coating presented in Figure 3B also exhibited a smaller apparent grain size than those prepared using the conditions of Experiments 4 and 5, as shown in Table 5.

Table 6 also presents the simulation results of the EIS data obtained from the SPC deposited coating/substrate systems. As verified in Nyquist diagrams (Figure 6B), only the coating/substrate system obtained from Experiments 2', 4', and 5'

Table 6 – Simulated results obtained from the EIS data for the DC and PC produced coating/substrate systems in NaCl 0.5 mol L⁻¹ (Figure 6), using the equivalent circuits presented in Figure 7.

Samples (Ω)	R_s (Ω cm ²)	R_{ct} (F cm ²)	C_{DL}	N (Ω cm ²)	R_f (F cm ²)	C_{DLf}	N_f (%)	Error	
Carbon steel	6.31	960.4	4.38×10^{-4}	0.746	-	-	-		
DC	Experiment 2	6.03	1151.5	1.24×10^{-5}	0.771	37.09	8.40×10^{-4}	0.779	0.59
	Experiment 3	5.28	1626.8	2.78×10^{-5}	0.886	44.98	1.51×10^{-4}	0.899	0.26
	Experiment 4	6.06	1401.4	2.14×10^{-4}	1.00	313.11	1.13×10^{-4}	0.876	0.02
	Experiment 5	6.65	1372.0	3.25×10^{-5}	1.00	212.17	1.94×10^{-4}	0.874	0.04
	Experiment 6	5.40	1102.5	3.42×10^{-5}	0.858	27.44	2.05×10^{-3}	0.834	0.16
	Experiment 2'	5.91	2376.5	1.31×10^{-4}	0.980	360.15	8.06×10^{-4}	0.873	0.11
Experiment 3'	4.70	735.0	5.43×10^{-4}	0.658	80.36	4.32×10^{-4}	0.858	0.08	
SPC	Experiment 4'	6.12	1641.5	3.85×10^{-4}	0.775	341.04	6.66×10^{-4}	0.832	0.16
	Experiment 5'	6.81	1323.0	2.86×10^{-4}	0.829	155.82	7.24×10^{-4}	0.761	0.28
	Experiment 6'	4.47	519.4	1.78×10^{-3}	0.758	136.71	6.97×10^{-4}	0.848	0.02

showed higher R_{ct} and lower C_{DL} values than the bare carbon steel substrate, indicating a higher anticorrosive performance in the studied medium (0.5 mol L⁻¹ NaCl). Similar to the results verified for the DC coatings, the film presenting the best anticorrosive performance among the SPC coating/substrate systems was obtained using $j_c = 267 \text{ A m}^{-2}$ (Experiment 2'), which showed lower Sn content ($2.80 \pm 0.41\%$ wt.) when compared to the coatings produced under the conditions of Experiments 4' and 5' (Table 3). Once more, it is probable that the minor defects (cracks and clusters) on the surface of the coatings presented in Figures 4C and 4D (Experiments 4' and 5', respectively) affected their ability to protect the substrate in the studied aggressive medium. Additionally, the coating prepared using $j_c = 267 \text{ A m}^{-2}$ (Experiment 2') presented the smallest apparent grain size among the SPC coatings. These results indicate that the composition of the coating may not be the only factor that must be considered for corrosion protection.

Based on these results, the cross-sections of the DC and SPC coating/substrate systems presenting the best anticorrosive performances (respectively, Experiment 3 using the DC process and Experiment 2' using the SPC process) were also evaluated using SEM and EDS analyses. Figure 8 shows these cross-section micrographs.

It is noted that the thickness value observed for the DC coating (Figure 8A) seems to be about 60% higher than the value shown in Table 3, while few differences are noted for the SPC one (Figure 8B). Thickness evaluation of an electrodeposited film is always a complex task since the film is not perfectly smooth, and different thicknesses at

different places may be measured. The cut of the samples for cross-section SEM analysis shown in Figure 8 was carried out to permit the evaluation of their central part, discarding their borders (Section 2.4.1, Experimental Procedures). The evaluation of the coatings' thickness using only these images could not reach representative values, although they could be valid for direct comparison, which is the aim here. On the other hand, the thickness values presented in Table 3 were calculated based on Equation 3, which considers the mass deposited over the whole electrode area. Although valid, the thickness values presented in Table 3 must be used with care because the densities of the material in bulk and thin film forms are usually different⁵⁶.

Figure 8A confirms that a compact coating, without apparent defects, was produced by DC electrodeposition using $j = 80 \text{ A m}^{-2}$, which ratifies that the morphology of this coating has contributed to the improved anticorrosive performance obtained in this case (Table 6). Elemental analysis of this coating using EDS mapping (Figure 8B) was also performed to verify the distribution of copper and tin in the film. The iron and carbon detected in the mapping are part of the substrate composition (carbon steel). Carbon can also be observed on the top of Figure 8B due to the resin used to embed the samples. It is possible to verify that the coating is composed mainly of copper and small traces of tin, uniformly distributed throughout it. This result agrees with the composition obtained by the ICP-OES analysis, which showed that the film produced had a higher average copper content than tin ($97.59 \pm 0.15\%$ wt. Cu and $2.41 \pm 0.18\%$ wt. Sn, Table 3). It is also interesting to note that

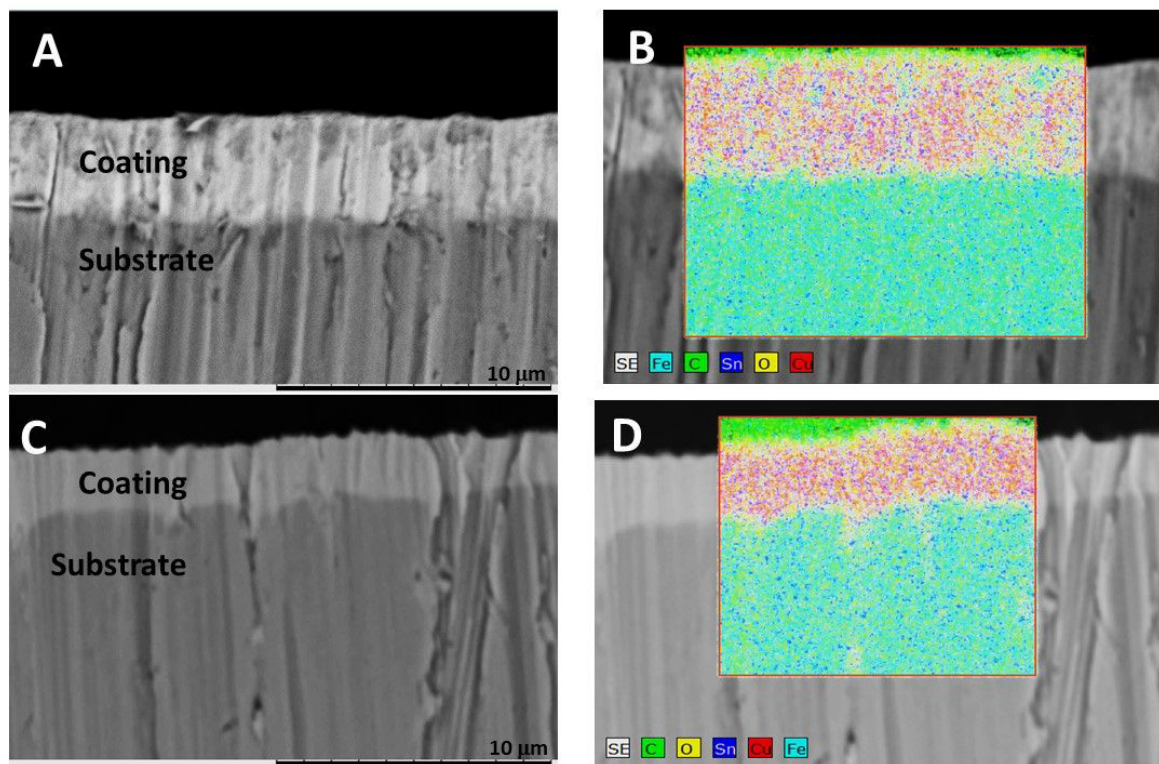


Figure 8. Cross-section images and EDS mapping analysis of the coatings produced using $j = 80 \text{ A m}^{-2}$ (Experiment 3; A, B) and $j_c = 167 \text{ A m}^{-2}$ (Experiment 2'; C, D).

small amounts of oxygen and iron are also present in the coatings. The presence of iron oxide on the coating/interface has already been detected in the literature⁵⁷. It can be related to the oxidation of the substrate in contact with the deposition bath during the electrodeposition process ($\text{Fe} + \text{Cu}^{2+} \rightarrow \text{Fe}^{2+} + \text{Cu}$). Under the conditions used in the present work, the formation of iron oxide could have probably continued during the DC plating process, enhanced by the surface alkalization due to the HER. The inclusion of iron oxide particles in electrodeposited metallic alloy coatings likely increased the corrosion resistance of these coatings by filling the holes formed during the deposition process⁵⁸. Therefore, the presence of iron oxide inside the coating could have contributed to the anticorrosive protection observed for this coating. However, it is important to mention that a diffraction line related to iron oxide was not verified in the diffractogram obtained for this coating (Figure 5A).

A compact coating, presenting a more irregular surface, was obtained when SPC deposition was used under Experiment 3' conditions (Figure 8C), which confirms the influence of the coating morphology in its anticorrosive performance. The EDS analysis also shows a copper-rich coating presenting well-distributed small tin amounts, agreeing with the ICP analysis shown in Table 3. Oxygen was also observed in this coating, mainly in the coating/substrate interface due to substrate oxidation. This element was also found on the top of the coating. Nevertheless, there was no detection of iron inside this coating. The presence of oxygen on the top of the sample can be related to micropores in the coatings, through which the oxygen on the interface could have migrated. Also, it is not possible to discard the presence of tin or copper oxides on the surface of the coating^{53,59}, which could also affect the anticorrosive performance of this system. However, X-Rays analysis did not detect these compounds (Figure 5B).

3.4.4. Comparison between the selected DC and SPC coating/substrate systems

The best anticorrosive coating/substrate systems produced using DC and PC processes were obtained under Experiments 3 (DC, $j = 80 \text{ A m}^{-2}$) and 2' (SPC, $j_c = 167 \text{ A m}^{-2}$) conditions, respectively. These coatings presented similar chemical composition (Table 3) and compact morphology (Figure 8).

However, the DC coating showed an apparent grain size smaller than the SPC one (Table 5). Comparing their protection behavior, Table 6 shows that the system prepared under the conditions of Experiment 2' presented higher R_{ct} and R_f values than that obtained from Experiment 3. However, the C_{DL} and C_{DLf} values of this system were higher than those of the DC-produced coating, suggesting a greater oxidation tendency of the SPC coating/substrate system compared to the DC system.

The results concerning the corrosion current density (j_{corr}), related to the corrosion velocity, and the corrosion potential (E_{corr}), obtained using polarization curves and Tafel extrapolation of these coating/substrate systems, are shown in Table 7. Both coating/substrate systems presented more cathodic corrosion potentials than the bare substrate in the same medium ($E_{corr(steel)} = -0.745 \text{ V}_{SCE}$), confirming that the produced layers may act as protective coatings. Moreover,

it is noted that the SPC system (Experiment 2') presents a slightly higher j_{corr} value when compared to the DC one (Experiment 3).

Based on all of these results, the anticorrosive performances of both coating/substrate systems were evaluated by EIS concerning their long-term exposure to the aggressive environment after being immersed in NaCl 0.5 mol L⁻¹ for 24h. Figure 9 shows the Nyquist diagrams for these coatings after 1h and 24h exposure in the corrosive medium. It can be observed, in Figure 9A, that the diameters of the capacitive loops for the DC-produced Cu-Sn coating/substrate systems obtained after 1 h and 24 h of immersion in NaCl 0.5 mol L⁻¹ were very similar. This result suggests that the evolution of the corrosive process with the exposure time was avoided and that this coating could protect the carbon steel substrate after 24 h in contact with the corrosive medium.

On the other hand, the diameter of the capacitive loop obtained for the SPC-produced Cu-Sn coating/substrate system (Figure 9B) decreased after 24h of immersion in the corrosive medium compared to the same sample analyzed after 1 h of exposure. This result suggests that the SPC coating may not maintain the same protection to the substrate after 24 h immersed in the 0.5 mol L⁻¹ NaCl solution. Nevertheless,

Table 7. j_{corr} and E_{corr} values obtained from the Tafel extrapolation of the polarization curves in NaCl 0.5 mol L⁻¹ for the coating/substrate systems prepared under the conditions of Experiments 3 (DC, $j = 80 \text{ A m}^{-2}$) and 2' (SPC, $j_c = 167 \text{ A m}^{-2}$).

Experiment 3 (DC)		Experiment 2' (SPC)	
j_{corr} (A cm ⁻²)	E_{corr} (V _{SCE})	j_{corr} (A cm ⁻²)	E_{corr} (V _{SCE})
1.42×10^{-5}	-0.660	3.33×10^{-5}	-0.664

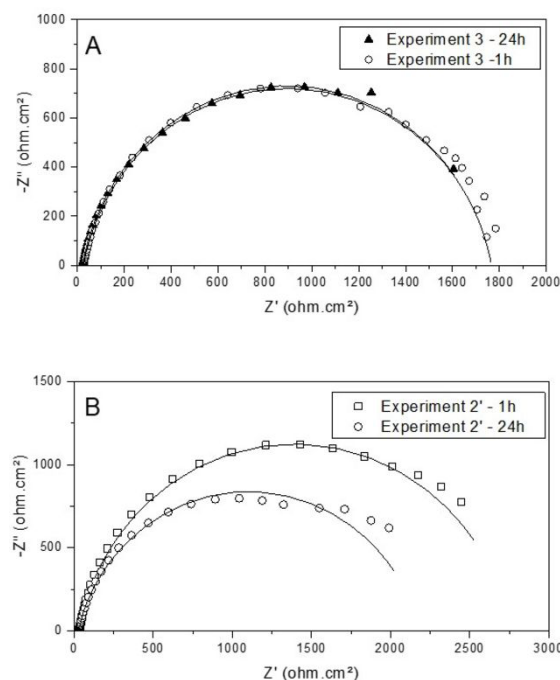


Figure 9. Nyquist diagram for the Cu-Sn coating/substrate obtained using the conditions of (A) Experiment 3 and (B) Experiment 2', after 1 h and 24 h of immersion in NaCl 0.5 mol L⁻¹

the capacitive loop of this coating after 24 h immersed in the corrosive medium continued higher than that verified for the DC coating analyzed under the same condition.

The circuit shown in Figure 7B was also used to simulate the EIS data for the SPC and DC-produced systems after 24 h of immersion in the aggressive medium, and Table 8 shows the R_{ct} and C_{DL} values obtained after these simulations. It is possible to see that the R_{ct} and C_{DL} values for the DC coating/substrate system immersed in the NaCl medium for 24h were close to those obtained for the coating after only 1 h of immersion, confirming the results of Figure 9A. The same table shows a decrease of approximately 15% in the R_{ct} value and an increase of approximately 26% in the C_{DL} value of the SPC coating/substrate system analyzed after 24 h of immersion in NaCl 0.5 mol L⁻¹ when compared to the results of the same system after 1 h of immersion in the corrosive medium.

It is interesting to note that the R_{ct} value for the system produced under the conditions of Experiment 2', after 24h

of exposure to the corrosive medium, is still higher than the system prepared by DC electrodeposition analyzed after the same immersion time. However, different from what was observed for the DC system, the solution related to the SPC system was yellowish after 24 h of exposure in the aggressive medium, indicating that Fe (III) ions were probably produced due to the substrate corrosion process.

The long-time exposure results can be related to the morphology of these coatings. Therefore, Figure 10 presents the cross-section and EDS analyses of the coatings produced under Experiments 3 and 2' conditions performed after 24 h of exposure to the corrosive medium. The analyzed region of these samples can be considered similar to those observed in the cross-section analysis shown in Figure 8, as the cut was performed to exhibit the central part of the samples in both cases.

Both films shown in Figure 10 present irregular surfaces, suggesting that the long-term exposure to the aggressive environment might have caused damage to the coatings.

Table 8 - Simulated results obtained from the EIS data obtained for the coating/substrate systems, produced under the conditions of Experiments 3 and 2' (DC and PC produced systems, respectively), after 1 h and 24 h of exposure to the corrosive medium and using the equivalent circuits presented in Figure 7B.

Experiment	Immersion time	R_s (Ω)	R_{ct} (Ω cm ²)	C_{DL} (F cm ²)	N	R_f (Ω cm ²)	C_{DLf} (F cm ²)	N_f	Error (%)
3	1 h	5.28	1626.8	2.78x10 ⁻⁵	0.886	44.98	1.51x10 ⁻⁴	0.899	0.26
	24 h	4.73	1616.0	3.08x10 ⁻⁵	0.990	122.50	4.11x10 ⁻³	0.889	0.08
2'	1 h	5.91	2376.5	1.31x10 ⁻⁴	0.980	360.15	8.06x10 ⁻⁴	0.873	0.11
	24 h	5.06	2009.0	1.76x10 ⁻⁴	0.954	151.9	9.48x10 ⁻⁴	0.840	0.34

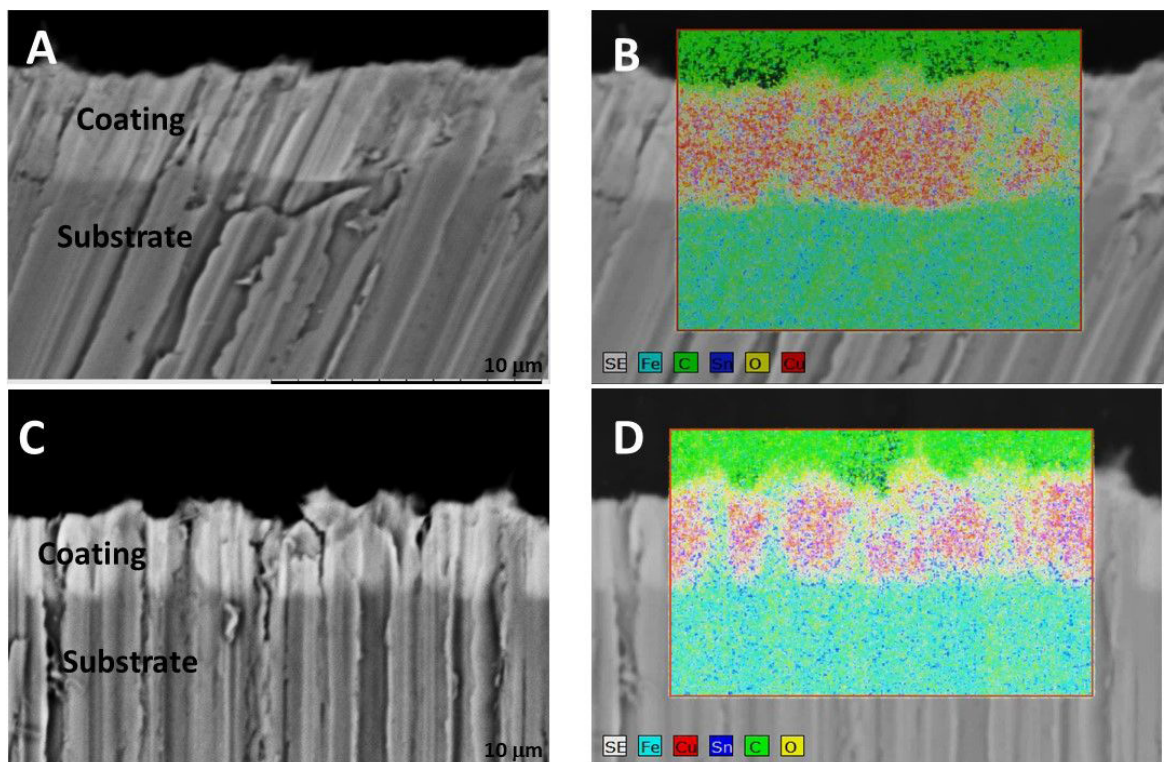


Figure 10. Cross-section images and EDS mapping analysis of the coatings produced using $j = 80$ A m⁻² (Experiment 3, A, B) and $j_c = 167$ A m⁻² (Experiment 2', C, D) after 24 h of immersion in NaCl 0.5 mol L⁻¹.

There is a slight increase in the thickness of the DC coating (Experiment 3), shown in Figure 10A, which can be related to the presence of the metallic oxides in the coating, including the iron oxide (Figure 10B). However, there is no coating degradation, which agrees with the Nyquist diagram shown in Figure 9A. This result suggests that this coating maintained its anticorrosive performance during the exposure period used in the present studies. The presence of iron oxide in the original sample, filling the pores of the coating, likely contributed to this performance⁵⁸.

On the other hand, the coating produced using the SPC process shows a more significant deterioration after 24 h of exposure to the corrosive medium (Figure 10C) compared to the DC coating (Figure 10A). The SPC coating presents cracks and defects, and the presence of iron oxide in almost all of the coating confirms the electrolytic attack of the substrate. This result agrees with the Nyquist diagram presented in Figure 9B and the increase in the C_{DL} value of the SPC system, indicating that this coating may not be able to protect the substrate in 0.5 mol L⁻¹ NaCl solution after 24 h of immersion.

4. Conclusions

The chemical, morphological and anticorrosive properties of electrodeposited Cu-Sn alloy coatings on steel substrate from a sodium citrate-based electrolyte were evaluated. The first part of this work dealt with the effects of the current mode (DC and SPC) and the applied current density (j or j_c) in these properties.

Initially, voltammetric experiments indicated that the bath composition and pH used in this work would favor the deposition of low-Sn Cu-Sn alloy coatings. In fact, coatings containing at least 91.97±0.15%wt. Cu were electrodeposited on carbon steel using the studied electrolytic bath, independent of the current mode. When the current modes were compared, for the same $j = j_m$ value, higher cathodic efficiency values were obtained using the SPC process, and the effect of HER parallel reaction could only be noted when $j_c = 667.0$ A m⁻² was used. Also, the increase in j_c caused polarization in the copper deposition process, favoring the tin reduction and confirming the effect of the pulse current in the alloy electrodeposition from this bath.

Coatings presenting granular cluster morphologies and few defects were obtained using both DC and SPC processes. However, those prepared under the conditions of Experiment 6 (DC, using $j = 200$ A m⁻²) showed flower-like structures on the film surface. The main phase formed in the coatings produced using both current modes was Cu₆Sn₅, although the phase Cu₃Sn was also found for some of the produced DC coatings. The smallest apparent grain size was observed for the DC coating prepared under the conditions of Experiment 3 ($j = 80$ A m⁻²).

Although showing %wt. Sn content smaller than that of commercial bronze (~5%wt. Sn), the coating/substrate systems produced using the conditions of Experiment 3 (DC and $j = 80$ A m⁻²) and Experiment 2' (SPC and $j_c = 167$ A m⁻²) showed the best anticorrosive performances among the Cu-Sn samples. Their cross-section images confirmed that compact coatings were prepared under these conditions, showing no defects. However, after 24 h of exposure to the corrosive

medium, the SPC coating deteriorated, and it is possible to suggest that only the Experiment 3 system can be used in long-term anticorrosive applications. The presence of iron oxide in the original coating likely contributed to filling the pores of the coating, avoiding its degradation.

Likely, the frequency value used in this work could have caused only small differences in the morphology and chemical compositions observed for the DC and SPC coatings. Therefore, in the second part of this work, the frequency and the duty cycle will be varied, and all the studied properties will be further evaluated.

5. Acknowledgments

This study was financed in part by the “Coordenação de Aperfeiçoamento de Pessoal de Nível Superior - Brasil (CAPES)” - Finance Code 001.

The authors would also like to thank the Rio de Janeiro Research Foundation (FAPERJ), the Brazilian National Research Council (CNPq), the State University of Rio de Janeiro (UERJ), and the Prociência Program for financial support. Additionally, we would like to thank Isaac Mallet (LabMEV/UERJ) for the SEM analysis, Diego Barros (LEAMS/ UERJ) for the chemical analysis, and Camila Santos Silva (LEC/UERJ) for the additional electrochemical analysis.

6. References

- Landolt D. Electrochemical and materials science aspects of alloy deposition. *Electrochim Acta*. 1994;39(8-9):1075-90.
- Silva FLG, Garcia JR, Cruz VGM, Luna AS, do Lago DCB, Senna LF. Response surface analysis to evaluate the influence of deposition parameters on the electrodeposition of Cu-Co alloys in citrate medium. *J Appl Electrochem*. 2008;38(7):1763-9.
- Sürme Y, Gürten AA, Bayol E, Ersoy E. Systematic corrosion investigation of various Cu-Sn alloys electrodeposited on mild steel in acidic solution: dependence of alloy composition. *J Alloys Compd*. 2009;485(1-2):98-103.
- Carlos I, Bidoia E, Pallone E, Almeida M, Souza C. Effect of tartrate content on aging and deposition condition of copper-tin electrodeposits from a non-cyanide acid bath. *Surf Coat Tech*. 2002;157:14-8.
- Silva PS, Senna LF, Lago DCB. Cu-Sn coatings produced using environmentally non-aggressive electrolyte containing sodium tartrate. *Mater Res*. 2017;20(Suppl. 2):667-75.
- Han C, Liu Q, Ivey DG. Nucleation of Sn and Sn-Cu alloys on Pt during electrodeposition from Sn-citrate and Sn-Cu-citrate solutions. *Electrochim Acta*. 2009;54(12):3419-27.
- Pu W, He X, Ren J, Wan C, Jiang C. Electrodeposition of Sn-Cu alloy anodes for lithium batteries. *Electrochim Acta*. 2005;50(20):4140-5.
- Perger G, Robinson P. Pulse plating-retrospects and prospects. *Met Finish*. 1979;77:17-9.
- Chandrasekar M, Pushpavanam M. Pulse and pulse reverse plating - conceptual, advantages and applications. *Electrochim Acta*. 2008;53(8):3313-22.
- Puippe JC, Leaman F. Theory and practice of pulse plating. 1st ed. Orlando: American Electroplaters and Surface Finishers Society; 1986.
- Zanella C, Xing S, Deflorian F. Effect of electrodeposition parameters on chemical and morphological characteristics of Cu-Sn coatings from a methanesulfonic acid electrolyte. *Surf Coat Tech*. 2013;236:394-9.
- Walsh F, Low C. A review of developments in the electrodeposition of tin-copper alloys. *Surf Coat Tech*. 2016;304:246-62.
- Slupska M, Ozga P. Electrodeposition of Sn-Zn-Cu alloys from citrate solutions. *Electrochim Acta*. 2014;141:149-60.

14. Brenner A. *Electrodeposition of alloys: principles and practice*. New York: Academic Press; 1963.
15. Correia AN, Façanha MX, Lima-Neto P. Cu–Sn coatings obtained from pyrophosphate-based electrolytes. *Surf Coat Tech*. 2007;201:7216-21.
16. Balachandra J. Electrodeposition of copper-tin alloys from fluoborate bath. *Curr Sci*. 1951;20:99.
17. Nickchi T, Ghorbani M. Pulsed electrodeposition and characterization of bronze-graphite composite coatings. *Surf Coat Tech*. 2009;203:3037-43.
18. Lima TG, Rocha BCCA, Braga AVC, Lago DCB, Luna AS, Senna LF. Response surface modeling and voltammetric evaluation of Co-rich Cu–Co alloy coatings obtained from glycine baths. *Surf Coat Tech*. 2015;276:606-17.
19. Jung M, Lee G, Choi J. Electrochemical plating of Cu–Sn alloy in non-cyanide solution to substitute for Ni undercoating layer. *Electrochim Acta*. 2017;241:229-36.
20. Pewnim N, Roy S. Electrodeposition of tin-rich Cu–Sn alloys from a methanesulfonic acid electrolyte. *Electrochim Acta*. 2013;90:498-506.
21. Bengoa LN, Pary P, Conconi MS, Egli WA. Electrodeposition of Cu–Sn alloys from a methanesulfonic acid electrolyte containing benzyl alcohol. *Electrochim Acta*. 2017;256:211-9.
22. Rode S, Henninot C, Vallières C, Matlosz M. Complexation chemistry in copper plating from citrate baths. *J Electrochem Soc*. 2004;151(6):C405-11.
23. Green T, Russell A, Roy S. The development of a stable citrate electrolyte for the electrodeposition of copper-nickel alloys. *J Electrochem Soc*. 1998;145(3):875-81.
24. Bonhote C, Landolt D. Microstructure of Ni/Cu multilayers electrodeposited from a citrate electrolyte. *Electrochim Acta*. 1997;42(15):2407-17.
25. Cherkaoui M, Chassaing E, Quang KV. Pulse plating of Ni–Cu alloys. *Surf Coat Tech*. 1988;34(3):243-52.
26. Gomez E, Labarta A, Llorente A, Valles E. Characterisation of cobalt/copper multilayers obtained by electrodeposition. *Surf Coat Tech*. 2002;153(2-3):261-6.
27. Survila A, Mockus Z, Juškėnas R, Jasulaitienė V. Electrodeposition of Sn and Co coatings from citrate solutions. *J Appl Electrochem*. 2001;31(10):1109-16.
28. Sun W, Ivey D. Development of an electroplating solution for codepositing Au–Sn alloys. *Mater Sci Eng B*. 1999;65(2):111-22.
29. Yapontseva Y, Kublanovsky V. Electrodeposition of tin (II) from citrate complexes. *Turk J Chem*. 2019;43:73-83.
30. Heidari G, Khoie SM, Abrishami ME, Javanbakht M. Electrodeposition of Cu–Sn alloys: theoretical and experimental approaches. *J Mater Sci Mater Electron*. 2015;26(3):1969-76.
31. Ding L, Chen C, Li Q, Yuan J, Li H, Xue Y, et al. Process and theoretical research on electroplating Cu–Sn alloys of low Sn. *J Appl Electrochem*. 2021;51(9):1287-99.
32. Mallik M, Mitra A, Sengupta S, Das K, Ghosh RN, Das S. Effect of current density on the nucleation and growth of crystal facets during pulse electrodeposition of Sn–Cu lead-free solder. *Cryst Growth Des*. 2014;14(12):6542-9.
33. Tang W, Hu Y, Huang S. Fabrication of Sn–Cu alloy solder by pulse electroplating on the metalized Si wafer. *Met Mater Int*. 2012;18(1):177-83.
34. Souza TM, Lago DCB, Senna LF. Electrodeposition of Co-rich Cu–Co Alloys from sodium tartrate baths using direct (DC) and single pulsed current (SPC). *Mater Res*. 2019;22(3):e20180272.
35. Cullity BD. *Elements of X-rays diffraction*. 2nd ed. London: Addison-Wesley; 1978.
36. Hirschorn B, Orazem ME, Tribollet B, Vivier V, Frateur I, Musiani M. Determination of effective capacitance and film thickness from constant-phase-element parameters. *Electrochim Acta*. 2010;55(21):6218-27.
37. Chassaing E, Quang KV, Wiart R. Kinetics of copper electrodeposition in citrate electrolytes. *J Appl Electrochem*. 1986;16(4):591-604.
38. Aravinda C, Mayanna S, Muralidharan V. Electrochemical behaviour of alkaline copper complexes. *J Chem Sci*. 2000;112(5):543-50.
39. Han C, Liu Q, Ivey DG. Kinetics of Sn electrodeposition from Sn(II)–citrate solutions. *Electrochim Acta*. 2008;53(28):8332-40.
40. Gervasi C, Bimbi MF, Alvarez P. Characterization of anodic tin passive films formed in citrate buffer solutions. *J Electroanal Chem*. 2009;625(1):60-8.
41. Seruga M, Metikos-Hukovic M. Passivation of tin in citrate buffer solutions. *J Electroanal Chem*. 1992;334(1-2):223-40.
42. Gervasi C, Alvarez P, Bimbi MF, Folquer M. Comparative cyclic voltammetry and SEM analysis of tin electrodes in citrate buffer solutions. *J Electroanal Chem*. 2007;601(1-2):194-204.
43. Survila A, Mockus Z, Stase K. Kinetics of Sn and Co codeposition in citrate solutions. *Electrochim Acta*. 2000;46(4):571-7.
44. Chassaing E, Vu Quang K, Wiart R. Kinetics of copper electrodeposition in citrate electrolytes. *J Appl Electrochem*. 1986;16(4):591-604.
45. Meng G, Sun F, Wang S, Shao Y, Zhang T, Wang F. Effect of electrodeposition parameters on the hydrogen permeation during Cu–Sn alloy electrodeposition. *Electrochim Acta*. 2010;55(3):2238-45.
46. Landolt D, Marlot A. Microstructure and composition of pulse-plated metals and alloys. *Surf Coat Tech*. 2003;169:8-13.
47. Roy S, Landolt D. Effect of off-time on the composition of pulse-plated Cu–Ni alloys. *J Electrochem Soc*. 1995;142(9):3021-7.
48. Devaraj G, Guruviah S, Seshadri S. Pulse plating. *Mater Chem Phys*. 1990;25(5):439-61.
49. Juškėnas R, Mockus Z, Kanapekaitė S, Stalnionis G, Survila A. XRD studies of the phase composition of the electrodeposited copper-rich Cu–Sn alloys. *Electrochim Acta*. 2006;52(3):928-35.
50. Gerenot Y, Dymarskaya P, Eichis A. The structure of copper-tin galvanic deposits. *Prot Met*. 1967;3(4):395-400.
51. Gilles B. Grazing incidence diffraction: a review. In: 5th School on X-Ray Diffraction from Polycrystalline Materials; 1996 Oct 2-5; Frascati, Rome, Italy. Proceedings. Frascati: SIS Publications; 1996. p. 177-204.
52. Barbano EP, de Oliveira GM, de Carvalho MF, Carlos IA. Copper–tin electrodeposition from an acid solution containing EDTA added. *Surf Coat Tech*. 2014;240:14-22.
53. Ding L, Li Q, Cheng J, Yuan J, Wang Q, Xue Y, et al. The electrodeposition of low Sn imitation gold Cu–Sn alloy from EDTA tartrate double complexing agents. *J Appl Electrochem*. 2021;51(3):473-87.
54. Eliaz N, Venkatakrisna K, Hegde AC. Electroplating and characterization of Zn–Ni, Zn–Co and Zn–Ni–Co alloys. *Surf Coat Tech*. 2010;205(7):1969-78.
55. Subramanian B, Mohan S, Jayakrishnan S. Structural, microstructural and corrosion properties of brush plated copper–tin alloy coatings. *Surf Coat Tech*. 2006;201(3):1145-51.
56. Eckertová L. *Physics of thin films*. Boston: Springer; 1977. Thin film thickness and deposition rate measurement methods; p. 52-71.
57. Banerjee A, Dutta M, Bysakh S, Bhowmick AK, Laha T. A novel coating strategy towards improving interfacial adhesion strength of Cu–Sn alloy coated steel with vulcanized rubber. *Appl Surf Sci*. 2014;313:804-16.
58. Chandrappa K, Venkatesha T. Electrochemical bulk synthesis of Fe₃O₄ and α -Fe₂O₃ nanoparticles and its Zn–Co– α -Fe₂O₃ composite thin films for corrosion protection. *Mater Corros*. 2014;65(5):509-21.
59. Kharitonov DS, Kasach AA, Sergievich DS, Wrzesińska A, Bobowska I, Darowicki K, et al. Ultrasonic-assisted electrodeposition of Cu–Sn–TiO₂ nanocomposite coatings with enhanced antibacterial activity. *Ultrason Sonochem*. 2021;75:105593.